John von Neumann Institute for Computing

Computer Simulations of the Phase Behavior and Transport Phenomena in Multicomponent Melts

Jürgen Horbach, Subir K. Das, Hans Knoth, Kurt Binder

published in

NIC Symposium 2004, Proceedings,
Dietrich Wolf, Gernot Münster, Manfred Kremer (Editors),
John von Neumann Institute for Computing, Jülich,
NIC Series, Vol. **20**, ISBN 3-00-012372-5, pp. 215-225, 2003.

http://www.fz-juelich.de/nic-series/volume20

Computer Simulations of the Phase Behavior and Transport Phenomena in Multicomponent Melts

Jürgen Horbach, Subir K. Das, Hans Knoth, and Kurt Binder

Institut für Physik, Johannes Gutenberg–Universität Mainz
Staudinger Weg 7, 55099 Mainz, Germany
E-mail: {horbach, subir, knoth, kurt.binder}@uni-mainz.de

Computer simulations are used to investigate typical phenomena in dense liquids and glasses that stem from the mixing of several chemical components. Three case studies of multicomponent mixtures are presented: A binary symmetrical Lennard–Jones mixture is simulated by means of Monte Carlo (MC) and Molecular Dynamics (MD) methods in order to get a better understanding of the interplay of structure and dynamics at fluid–fluid unmixing transitions. Then we demonstrate that MD simulations in conjunction with neutron scattering experiments give evidence for the presence of intermediate range order (of the order of 6–7 Å) in sodium trisilicate. The structure that underlies the latter intermediate range order is important to understand the properties of the alkali diffusion in alkali silicate glasses. This is demonstrated in the last case study: A MD simulation of a ternary alkali silicate system gives insight into the microscopic origin of the so–called mixed alkali effect.

1 Introduction

It is one of the fundamental problems of statistical physics to understand the structure, dynamics, and phase behavior of multicomponent mixtures. Since the mixing of certain chemical components may lead to favorable material properties, the understanding of mixtures is also of basic interest for technological applications. An example is the production of tablets in pharmaceutical industry: It is of great importance for the efficacy of a tablet whether it is in a glass phase or a crystalline state, or whether for certain chemical components that tend to unmix, phase separation can be avoided by adding an additional component or by changing the production process of the tablet. In the following we present examples from our work where computer simulations are used to shed light on phenomena in multicomponent melts and glasses.

In our first example we consider a simple AB fluid mixture, a symmetrical Lennard-Jones (LJ) mixture, to study the transport properties near and at the coexistence states of a fluid–fluid unmixing transition. Thereby, the phase diagram and other thermodynamic properties are calculated by Monte Carlo simulations in the semigrandcanonical ensemble whereas structural and dynamic quantities are calculated by Molecular Dynamics (MD) simulations in the microcanonical ensemble. In the symmetrical LJ mixture the interactions between AA and BB pairs is identical and the possibility of the system to undergo a phase separation is driven by an AB interaction that is different from that between particles of the same species. It is clear that such a system does probably not give a realistic description of any real system, but it may exhibit essential features of fluid mixtures with respect to the unmixing transition in conjunction with structural and dynamic properties. It is important to understand first in detail simple model systems before one can continue to study more realistic ones. This is one of the merits of computer simulations that simplified models

can be studied to highlight universal properties of matter without getting lost in chemical details.

Secondly, we present the results of a "realistic" MD simulation of the sodium silicate (Na_2O)(3·SiO_2) [NS3] in the melt and the glass state and compare these results to those of a neutron scattering experiment. NS3 and other alkali silicates are paradigms for multi-component glass forming systems in which even at typical melt temperatures the mobility of the alkali ions exceeds that of the Si–O network by orders of magnitude[1]. In this context we are interested in the interplay between the structure and the fast sodium diffusion in NS3. It turns out that there is intermediate range order in the structure of NS3 that provides the existence of diffusion channels for the fast sodium diffusion. We demonstrate by this study how MD simulations can be used to elucidate the results of neutron scattering experiments. Since neutron scattering covers the observation of similar time and length scales as MD, one can directly compare simulation and experiment in this case. Thus, it is possible to check the accuracy of the simulation model by the neutron data, and then, one can make use of the detailed information obtained by the MD simulation to interprete the results of the neutron scattering experiment.

Thirdly, MD simulations of the ternary alkali silicate (0.5·Li_2O)(0.5· K_2O)(2·SiO_2) [LKS2] and the binary alkali silicates (Li_2O)(2·SiO_2) [LS2] and (K_2O)(2·SiO_2) [KS2] are used to investigate the microscopic origin of the so–called mixed–alkali effect (MAE). The MAE occurs in many vitreous alkali conductors that are mixtures of two alkali oxides (such as Li_2O and K_2O) and another oxide that forms a "stiff" network structure (such as the tetrahedral networks in SiO_2 and GeO_2). It is the phenomenon that the transport of the alkali ions in the latter ternary systems slows down drastically compared to the corresponding systems that contain only one alkali component[2]. In order to get insight into the MAE by MD, the simulation of rather large systems on relatively long time scales is required (see below). However, we demonstrate below that state of the art MD simulations on parallel computers shed light on the microscopic origin of the MAE.

2 Simulation of a Symmetrical Lennard–Jones Mixture

The symmetrical binary Lennard–Jones (LJ) mixture is the simplest case of a model that exhibits a fluid–fluid miscibility gap. It describes a system of point particles of type A and B that interact via the potential

$$u(r_{ij}) = 4\epsilon_{\alpha\beta}\left[(\sigma_{\alpha\beta}/r_{ij})^{12} - (\sigma_{\alpha\beta}/r_{ij})^{6}\right], \qquad r_{ij} = |\vec{r}_i - \vec{r}_j|, \qquad \alpha,\beta \in \mathrm{A},\mathrm{B}\ . \quad (1)$$

The Lennard–Jones parameters $\{\epsilon_{\alpha\beta}, \sigma_{\alpha\beta}\}$ are chosen as follows

$$\sigma_{\mathrm{AA}} = \sigma_{\mathrm{AB}} = \sigma_{\mathrm{BB}} = \sigma, \qquad \epsilon_{\mathrm{AA}} = \epsilon_{\mathrm{BB}} = \epsilon\ . \quad (2)$$

Moreover, units of length, temperature and energy are chosen by requiring that $\sigma = 1$, $\epsilon = 1$, and Boltzmann's constant $k_{\mathrm{B}} = 1$. In the Molecular Dynamics (MD) part, also the masses are chosen as $m_{\mathrm{A}} = m_{\mathrm{B}} = m = 1$ (of course, in the Monte Carlo (MC) part the masses are not considered). The mixture as described by the potential, Eq. (1), becomes nontrivial by choosing $\epsilon_{\mathrm{AB}} \neq \epsilon$. In our case we have chosen $\delta = \epsilon_{\mathrm{AB}}/\epsilon = 0.5 < 1$ which introduces the possibility of a phase separation because less energy is won for AB–pairs rather than for AA and BB pairs on a local scale. The potential is truncated and shifted to zero at $r_{ij} = 2.5\sigma$ and as a density we have chosen $\rho = 1$ which ensures that the system

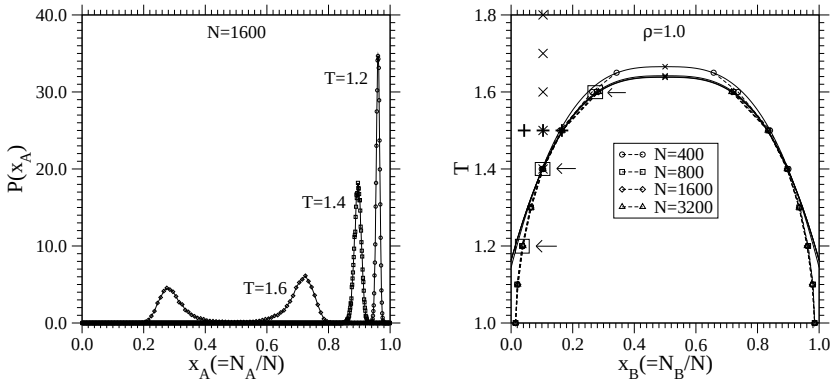

Figure 1. **Left panel:** Distribution function $P(x_{\rm A})$ for the relative concentration $x_{\rm A}$ of A particles for $N = 1600$ at $\mu = 0$ and the three temperatures indicated. **Right panel:** Phase diagram of the symmetrical binary Lennard–Jones mixture, including results for four choices of N, as indicated. Crosses at $x_{\rm B} = 0.10375$ and plus symbols at $T = 1.5$ and squares with arrows indicate paths in the $(T, x_{\rm B})$ plane for which the dynamical behavior was studied. From Das *et al.*[4].

exhibits neither any gas phases nor crystallization in the temperature range of interest, $1 \leq T \leq 2$.

In order to determine the phase diagram we use Monte Carlo simulations in the so–called semigrandcanonical ensemble in which the total particle number N, the volume V, the temperature T, and the chemical potential difference $\Delta\mu$ are fixed whereas the relative concentrations $x_{\rm A} = N_{\rm A}/(N_{\rm A} + N_{\rm B}) = N_{\rm A}/N$, $x_{\rm B} = N_{\rm B}/N$ are fluctuating variables[3]. In a semigrandcanonical move an identity change of the form $A \to B$ or $B \to A$ is tried for a randomly chosen particle. This move is accepted or rejected according to the standard Metropolis criterion whereby now apart from the energy change ΔE also the change in the chemical potential difference $\Delta\mu$ has to be taken into account in the Boltzmann factor. Due to the symmetry of our model, states at the coexistence curve are obtained by choosing $\Delta\mu = 0$ provided that one is below the critical temperature $T_{\rm c}$ of the unmixing transition. The location of the coexistence states can then be determined from the distribution function of the relative concentration $P(x_{\rm A})$ which is shown in the right panel of Fig. 1 for $T < T_{\rm c}$. As we see in the left panel of Fig. 1, at the low temperatures $T = 1.2$ and $T = 1.4$ we sample only one peak corresponding to an A rich phase. The reason for this behavior is that spontaneous transitions to the B rich phase are very unlikely, because the A rich and the B rich phase are separated from each other by a huge free energy barrier at low temperatures. This does not matter in the present case because we know *a priori* that the phase diagram must be completely symmetric due to the symmetry of the system.

The right panel of Fig. 1 shows the phase diagram for different system sizes of $N = 400, 800, 1600$, and 3200 particles. In this figure, the solid lines are fits with the expected power law $x_{\rm B}^{\rm crit} \pm x_{\rm B}^{\rm coex} = \hat{B}(1 - T/T_{\rm c})^{0.325}$ ($\hat{B}$ is a so–called "critical amplitude" and, due to the symmetry of the model, $x_{\rm B}^{\rm crit} = 1/2$) in order to estimate the critical temperature $T_{\rm c}$ of the unmixing transition. As we see, $N = 400$ does not allow a reliable estimate of $T_{\rm c}$, whereas for $N \geq 800$ the finite size effects are small and we obtain $T_{\rm c} = 1.638 \pm 0.005$.

The MC in the semigrandcanonical ensemble does not yield only the phase diagram but also well–equilibrated start configurations for MD simulations in the microcanonical ensemble. The thermodynamic states of these configurations are located exactly along

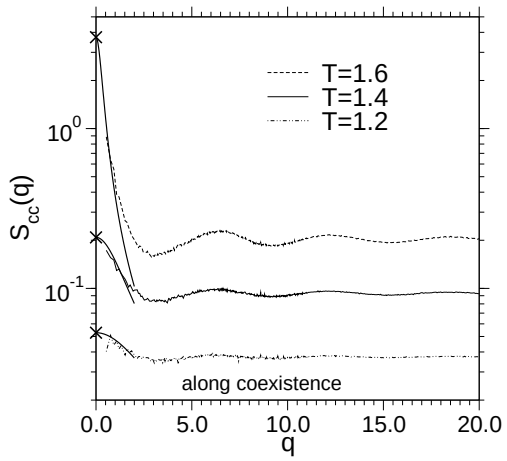

Figure 2. Concentration fluctuation structure factor $S_{\rm cc}(q)$ plotted vs. q, for three temperatures as indicated, choosing states along the coexistence curve (note the logarithmic scale of the ordinate). Crosses at the ordinate represent the "susceptibility" $k_BT\chi$ (see text), while the bold solid lines are fits to the Ornstein–Zernike equation (see text), which should hold at small q. From Das *et al.*[4].

the coexistence curve. We have calculated structural and dynamical quantities at three different paths by means of MD which are indicated in the right panel of Fig. 1: along the coexistence curve, at constant composition $x_{\rm B} = 0.10375$ (by changing the temperature), and at the isotherm $T = 1.5$, crossing the one–phase region up to the coexistence curve. All MD simulations were done with a system of $N = 1600$ particles. More details on the simulations can be found elsewhere[4].

A quantity of particular interest is the structure factor of the concentration fluctuations which can be written as[5]

$$S_{\rm cc}(q) = x_{\rm B}^2 S_{\rm AA}(q) + x_{\rm A}^2 S_{\rm BB}(q) - 2x_{\rm A}x_{\rm B}S_{\rm AB}(q), \tag{3}$$

where $S_{\alpha\beta}(q)$ ($\alpha, \beta \in \{\rm A, B\}$) denote the partial structure factors defined by

$$S_{\alpha\beta}(q) = \frac{1}{N}\sum_{k=1}^{N_\alpha}\sum_{l=1}^{N_\beta}\langle \exp[i\vec{q}\cdot(\vec{r}_k - \vec{r}_l)]\rangle \quad . \tag{4}$$

In Fig. 2 $S_{\rm cc}(q)$ is shown at three states along the coexistence line. While $S_{\rm cc}(r)$ is almost zero at low temperature, its amplitude for $q \to 0$ strongly increases as the critical point is approached. One expects that the Ornstein–Zernike equation holds, $S_{\rm cc}(q) = k_BT\chi/[1 + q^2\xi^2]$ with ξ being the correlation length and χ the susceptibility of concentration fluctuations. Fits with this equation are shown in Fig. 2. In these fits the susceptibility χ was not treated as a fit parameter but it was estimated from the semigrand-canonical MC by the fluctuation relation

$$S(q=0) = k_BT\chi = N\left\{\int_{1/2}^{1} x_{\rm A}^2 P(x_{\rm A})dx_{\rm A} - [x_{\rm A}^{\rm coex(1)}]^2\right\} \quad . \tag{5}$$

The values of $k_BT\chi$ are shown as crosses on the ordinate of Fig. 2. Note that one can never directly determine $k_BT\chi$ from a microcanonical MD simulation since there $S_{\rm cc}(q=0)$ is equal to zero because the total concentrations of A and B particles are fixed in this case

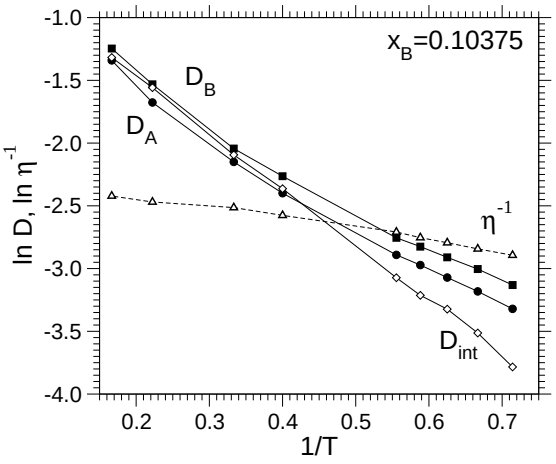

Figure 3. Logarithm of the selfdiffusion constants $D_{\rm A}$ (filled circles), $D_{\rm B}$ (filled squares), the interdiffusion constant $D_{\rm int}$ (open diamonds), and the inverse viscosity η^{-1} (open triangles) plotted vs. inverse temperature for the mixture at constant concentration $x_{\rm B} = 0.10375$. From Das *et al.*[4].

(one can only estimate $S_{\rm cc}(q = 0)$ by the rather inaccurate extrapolation $q \to 0^+$ in the microcanonical simulation).

We want to discuss now whether the static long–ranged concentration fluctuations as seen in Fig. 2 are accompanied by a qualitative change of the temperature dependence of transport coefficients in the vicinity of the coexistence line. To this end, we calculated the self–diffusion constants $D_{\rm A}$ and $D_{\rm B}$ from the mean squared displacement as well as the shear viscosity η and the interdiffusion constant $D_{\rm int}$ by the appropriate Green–Kubo formulas[5]. From Fig. 3 it is evident that all transport coefficients $D_{\rm A}$, $D_{\rm B}$, $D_{\rm int}$ and η^{-1} decrease as one lowers the temperature, but simple Arrhenius relations do not hold. In addition, we note that for the minority component the selfdiffusion constant always is a bit faster than for the majority component. The interdiffusion constant has a value which is hardly different from the selfdiffusion constants at high temperatures, but becomes appreciably smaller than the latter when one approaches the coexistence curve. One expects $D_{\rm int} \to 0$ if the path $x_{\rm B} = x_{\rm B}^{\rm crit} = 1/2$ would be chosen[3], so that one approaches the critical point, while the states considered in Fig. 3 are still strongly off–critical such that only a weak decrease of $D_{\rm int} \neq 0$ is observed.

The results for the viscosity allow a check of the Stokes–Einstein formula for the self-diffusion constants, $D_\alpha = k_B T/(2\pi\eta d_\alpha)$, d_α being the (effective) diameter of the corresponding particle species $\alpha \in \{{\rm A}, {\rm B}\}$ (note that we assume slip boundary conditions at the "surface" of the particles). If the Stokes–Einstein formula were strictly correct, one would expect $d_{\rm A} \approx \sigma_{\rm A} = 1$, $d_{\rm B} \approx \sigma_{\rm B} = 1$. It turns out that this would be a reasonable approximation for the A particles, while for the B particles the result rather is $d_{\rm A} \approx 0.8$[4].

Further simulation results on the symmetrical Lennard–Jones mixture can be found in a recent publication[4].

3 Intermediate Range Order in Binary Silicate Melts and Glasses

Alkali silicates are a paradigm for multicomponent glassforming systems in which even at typical melt temperatures the mobility of the alkali ions exceeds that of the Si–O network

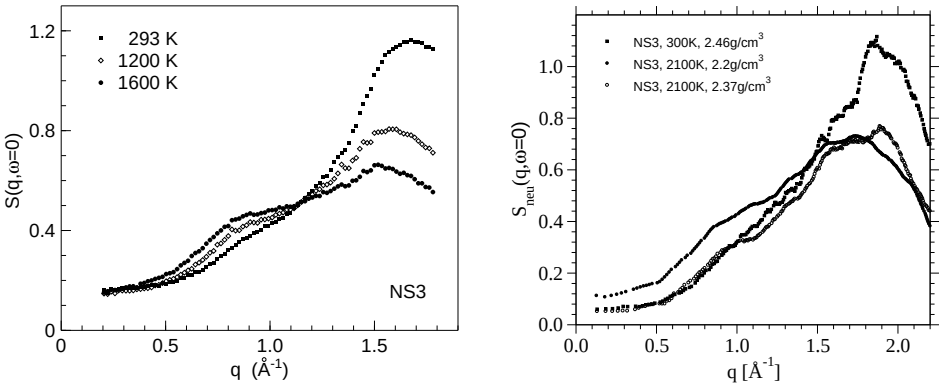

Figure 4. **Left panel:** The elastic structure factor of NS3 as obtained from a neutron scattering experiment for the three indicated temperatures. **Right panel:** The same quantity as obtained from the simulation at the indicated temperatures and densities. From Meyer et al.[8].

by orders of magnitude[1]. Although an explanation of such a high mobility of the alkali ions requires a profound knowledge of the structure, it has been one of the open questions how the alkali ions are built into the Si–O network. Indeed, we have shown recently by a MD simulation of sodium disilicate[6], (Na_2O)(2·SiO_2) [NS2], that the sodium ions move in a network of diffusion channels whereby the characteristic length scale of this network is related to a prepeak in the static structure factor at the wavenumber $q_1 = 0.95$ Å^{-1} corresponding to a length scale of $2\pi/q_1 \approx 6.6$ Å. Of course, it is not at all clear whether the potential that has been used to model the interactions in NS2[6,7] is accurate enough to give a realistic description of NS2 and other sodium silicates. Thus, the prepeak that has been found in the simulation could be just an artifact of the model potential.

Fortunately, recent neutron scattering experiments by A. Meyer *et al.* allow to check directly the accuracy of the simulation results[8]. The left panel in Fig. 4 shows the elastic structure factor $S_{\rm neu}(q, \omega = 0)$ from the latter experiments for (Na_2O)(3·SiO_2) [NS3] at the temperature $T = 300$ K corresponding to a glass state and at the two temperatures $T = 1200$ K and $T = 1600$ K where the system is in a liquid state. Note that one obtains to a good approximation a total static structure factor $S_{\rm neu}(q)$ from $S_{\rm neu}(q, \omega = 0)$ if one divides this quantity by the Debye–Waller factor $f(q)$. The experimental elastic structure factors clearly exhibit a shoulder around $q_1 = 0.9$ Å^{-1}. But surprisingly, this shoulder becomes less pronounced with decreasing temperature. At first glance this could mean that the structure that is associated with the feature at q_1 tends to dissappear at low temperature. The right panel of Fig. 4 shows the simulation results for $S_{\rm neu}(q, \omega = 0)$ at $T = 300$ K and $T = 2100$ K at the experimental densities $\rho = 2.46$ g/cm^3 and $\rho = 2.2$ g/cm^3, respectively. In addition, $S_{\rm neu}(q, \omega = 0)$ at $T = 2100$ K is shown at the density $\rho = 2.37$ g/cm^3. Obviously, the simulation gives a result which is qualitatively similar to that of the neutron scattering experiment. However, one also sees in Fig. 4 that the effect, that the feature at q_1 is more pronounced in the glass than in the melt, is smaller if one compares the curve for $T = 2100$ K at the density $\rho = 2.37$ g/cm^3 to that for $T = 300$ K. So it seems that it is due to a change in density and not due to the change in temperature that one obtains the anomalous behavior in $S_{\rm neu}(q, \omega = 0)$.

If one tries to interpret the $S_{\rm neu}(q, \omega = 0)$ as measured in neutron scattering one has to be aware of the fact that in a system with three different chemical components this quantity

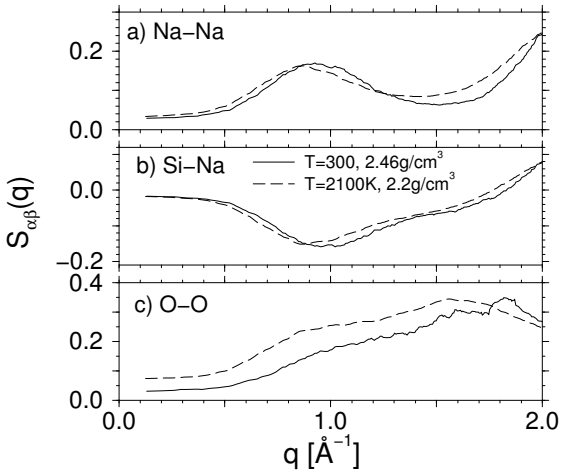

Figure 5. Partial structure factor for NS3 as obtained from the simulation at $T = 300$ K (solid lines) and at $T = 2100$ K (dashed lines) at the indicated densities. a) $S_{\mathrm{NaNa}}(q)$, b) $S_{\mathrm{SiNa}}(q)$, and c) $S_{\mathrm{OO}}(q)$. From Meyer *et al.*[8].

is a linear combination of six partial structure factors $S_{\alpha\beta}(q)$ (defined by Eq. (4)),

$$S_{\mathrm{neu}}(q,\omega=0) = \frac{f(q)}{x_{\mathrm{Si}}b_{\mathrm{Si}}^2 + x_{\mathrm{Na}}b_{\mathrm{Na}}^2 + x_{\mathrm{O}}b_{\mathrm{O}}^2}\left(b_{\mathrm{Si}}^2 S_{\mathrm{SiSi}}(q) + b_{\mathrm{Na}}^2 S_{\mathrm{NaNa}}(q) + b_{\mathrm{O}}^2 S_{\mathrm{OO}}(q) + \right.$$
$$\left. 2b_{\mathrm{Si}}b_{\mathrm{Na}}S_{\mathrm{SiNa}}(q) + 2b_{\mathrm{Si}}b_{\mathrm{O}}S_{\mathrm{SiO}}(q) + 2b_{\mathrm{Na}}b_{\mathrm{O}}S_{\mathrm{NaO}}(q)\right) \quad (6)$$

with $b_{\mathrm{Si}} = 0.4149 \cdot 10^{-12}$ cm, $b_{\mathrm{Na}} = 0.363 \cdot 10^{-12}$ cm, and $b_{\mathrm{O}} = 0.5803 \cdot 10^{-12}$ cm being the experimental neutron scattering length (note that we determined $f(q)$ in the simulation from the total coherent intermediate scattering function, see Ref.8). In the case of NS3 one does not have access to the $S_{\alpha\beta}(q)$ in the experiment, but these quantities can be easily determined in the simulation by means of Eq. (4). Fig. 5 shows $S_{\mathrm{NaNa}}(q)$, $S_{\mathrm{SiNa}}(q)$, and $S_{\mathrm{OO}}(q)$ at 300 K and 2100 K at the densities 2.46 g/cm^3 and 2.2 g/cm^3, respectively. Whereas in the elastic structure factor only a shoulder is present around q_1, a well–pronounced peak is found at q_1 in $S_{\mathrm{NaNa}}(q)$ and $S_{\mathrm{SiNa}}(q)$, and the latter two quantities exhibit only a weak temperature dependence. That one sees only a shoulder around q_1 in the total structure factor, is on the one hand due to cancellation effects of positive and negative contributions in the sum, Eq. (6) (see the negative amplitude of $S_{\mathrm{SiNa}}(q)$ around q_1) and on the other hand due to the behavior of $S_{\mathrm{OO}}(q)$ around q_1. The latter function gives the largest contribution in the total structure factor because oxygen is the majority species in NS3 (around 60% of the particles are oxygens). And it exhibits a similar behavior as $S_{\mathrm{neu}}(q,\omega=0)$: It shows only a shoulder around q_1 that becomes less pronounced at $T = 300$ K. The latter effect is not due to the lower temperature but due to the higher density at $T = 300$ K. Thus, in order to observe in scattering experiments of sodium silicates the feature at q_1, one has to either perform the measurements at high temperatures (because of the lower density compared to low temperatures) or one has to stretch the glass at room temperature.

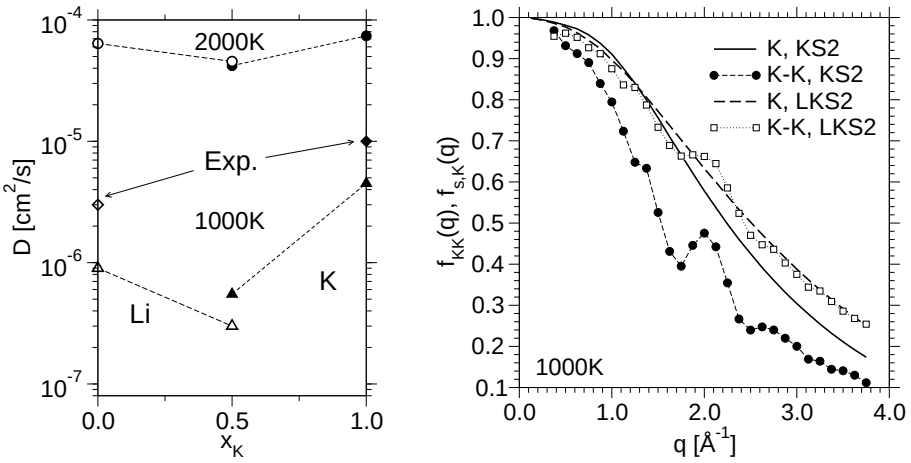

Figure 6. **Left panel:** Selfdiffusion constants of LS2, KS2, and LKS2 as a function of the potassium concentration $x_{\rm K}$ for the temperatures 2000 K and 1000 K as indicated. The diamonds correspond to experimental data at $T = 1000$ K[12]. **Right panel:** Debye–Waller factors $f_{\rm KK}(q)$ and Lamb–Mössbauer factors $f_{\rm s,K}(q)$ at $T = 1000$ K in KS2 and LKS2. From Knoth *et al.*[11].

4 The Mixed–Alkali Effect in Ternary Silicate Melts and Glasses

At the end of the 19th century the so–called thermometer effect was discovered. At that time, most of the thermometers were made of "Thüringer Glas" which is silicate glass that contains (among other oxides) the two alkali oxides Na_2O and K_2O. These thermometers had an unwished property if they were heated up too much: If the calibrated thermometer was put into boiling water and then some time later into ice, it showed -0.5°C instead of 0°C. The thermometer allowed again an accurate measurement at zero temperature if it was stored at room temperature for several months. In 1883 Weber found the solution to the thermometer problem: The thermometer effect is strongly diminished if the thermometer glass has only one alkali component[9].

The thermometer effect is an example of the so–called mixed alkali effect (MAE) that appears in many glassformers with two mobile alkali components (apart from silicates also in phosphates, borates etc.)[2]. It is the phenomenon that the self diffusion constants of the alkali ions in a system with two mobile alkali components may be orders of magnitude smaller than in the corresponding systems with only one alkali component. The MAE is very pronounced well below the glass transition temperature $T_{\rm g}$ (i.e. the temperature where the shear viscosity has a value of 10^{13} Poise) whereas at typical melt temperatures the diffusion constant decreases only by a factor of 2 or 3 in the mixed alkali system.

Many efforts have been undertaken to understand the MAE[2]. However a microscopic theory of the MAE is still lacking. In principle, MD simulations are well–suited to shed light on the microscopic origin of the MAE. But one is confronted with the aforementioned problem that the MAE is only visible at very low temperatures in a pronounced way where also the time scale for the diffusion dynamics of the mobile alkali ions exceeds the time scale that can be spanned by the simulation. Moreover, in the glass state the matrix atoms (i.e. Si and O) are not in equilibrium anymore and one has to be aware of non–eqilibrium effects (aging processes). We have also seen in Section 3 that the stucture of typical alkali silicate glasses exhibits features at relatively large (nanoscopic) length scales requiring the simulation of a relatively large system.

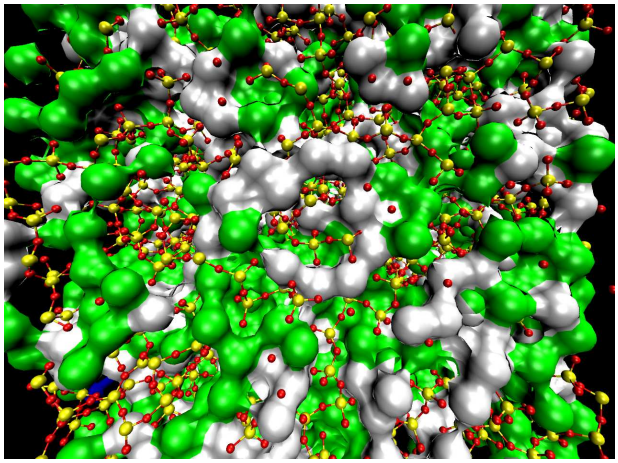

Figure 7. Snapshot of LKS2 at $T = 1000$ K. The green and silver spheres that are connected to each other figure the K and Li atoms, respectively. The Si–O network is drawn by yellow (Si) and red (O) spheres that are connected to each other by covalent bonds shown as sticks between Si and O spheres. From Knoth *et al.*[11].

We have done large scale MD simulations to study the alkali silicate systems $(Li_2O)(2{\cdot}SiO_2)$ [LS2], $(K_2O)(2{\cdot}SiO_2)$ [KS2], and $(0.5{\cdot}Li_2O)(0.5{\cdot}K_2O)(2{\cdot}SiO_2)$ [LKS2]. As a model potential we use the pair potential by Habasaki *et al.*[10] which has been parametrized by means of *ab initio* calculations and which shows good agreement with experimental data with respect to many static and dynamic quantities. The simulations were done for a system of $N = 8064$ particles (this system size was also used in the simulations of NS3 presented in Section 3). The two temperatures 2000 K and 1000 K are considered in the following where the system was first relaxed at constant pressure ($p = 0$) for 3.3 ns (2 million time steps) and 82 ns (50 million time steps), respectively, followed by production runs in the microcanonical ensemble over 3.3 ns and 8.2 ns, respectively. Whereas at $T = 2000$ K the system was fully equilibrated, at $T = 1000$ K the system was in a non–equilibrium state where only the alkali atoms show diffusive behavior. However, the long relaxation run at $T = 1000$ K was necessary to study aging processes in the Si–O network that may affect the alkali diffusion. More information on the simulation can be found elsewhere[11].

The left panel of Fig. 6 shows the selfdiffusion constants for the different systems as a function of the potassium concentration $x_K = N_K/N$. We can infer from this figure that our model exhibits at 2000 K and 1000 K the MAE. Whereas the MAE is very small at 2000 K, at 1000 K the MAE extends over about a factor of 3 in the case of Li and about one order of magnitude in the case of K. Also shown in the figure are experimental data for LS2 and KS2 at $T = 1000$ K[12], and we see that our simulation is in fair agreement with these data.

But what is the microscopic origin of the MAE in our model of LKS2? It turns out that the local dynamics of the alkali ions in LKS2 is qualitatively different from that in LS2 and KS2. And this is due to a different coupling of the "fast" alkali motion to the motion of the Si–O network. As we have shown recently[6] the motion of the alkali ions can be described by the hopping from one alkali site to another whereby these sites are located in a network of channels. In the case of a completely frozen Si–O network also the location

of the alkali sites would be frozen and the diffusivity of the alkali ions would be very small because it is the existence of fluctuations in the Si–O network that enables the opening of the channels. The important point is now to analyze how localized correlations between alkali sites are compared to the motion of single alkali ions. And this is quantified by means of the Debye–Waller factor $f_{\mathrm{KK}}(q)$ and the Lamb–Mössbauer factor $f_{\mathrm{s,K}}(q)$ which are shown for KS2 and LKS2 at $T = 1000$ K in the right panel of Fig. 6. In KS2 $f_{\mathrm{KK}}(q)$ decays much faster than $f_{\mathrm{s,K}}(q)$ which means that the correlations between potassium sites is much less localized than the one–particle potassium motion (note that the same behavior is found in LS2 at $T = 1000$ K). In contrast to that in LKS2 both quantities show a similar decay. In addition one can show[11] that it is very unlikely at the relatively low temperature $T = 1000$ K that sites for different alkali ions are exchanged, i.e. a Li ion does not hop on a K site and a K ion does not hop on a Li site. The interpretation that emerges is as follows: The mixing of different alkali components leads to a stiffening of the correlations between the alkali sites (these are as localized as the one–particle alkali motion itself) and thus the alkali ions are more strongly bound to their sites.

How are the alkali ions distributed in the system in LKS2? This is illustrated in the snapshot, Fig. 7. One can infer from this snapshot that the alkali ions are not homogeneously distributed but in the form of a network of channels in the SiO_2 matrix. Thereby, one can identify subnetworks of channels for the Li and the K ions. In fact, diffusion of the alkali ions takes place in "channels" between these subnetworks. The mechanism of this channel diffusion is given in detail in Ref. 11.

Acknowledgments

We thank A. Meyer (TU München) and W. Kob (Université Montpellier II) for a fruitful collaboration. S. K. D. was supported by the Deutsche Forschungsgemeinschaft (DFG) grant N$^{\mathrm{o}}$ Bi314–18 (SPP1120), J. H. by the DFG grant N$^{\mathrm{o}}$ HO2231/2–1, and H. K. by the Bundesministerium für Forschung und Technologie (BMBF) grant No. 03N6015. We are particularly grateful to the NIC Jülich for generous allocations of computer time.

References

1. J. R. Johnson, R. H. Bristow, and H. H. Blau, J. Am. Ceram. Soc. **34**, 165 (1951); Y. P. Gupta and T. B. King, Trans. Metall. Soc. A.I.M.E. **237**, 1701 (1966); M. Braedt and G. H. Frischat, Phys. Chem. Glasses **29**, 214 (1988).
2. D. E. Day, J. Non–Cryst. Sol. **21**, 343 (1976); M. D. Ingram, Phys. Chem. Glasses **28**, 215 (1987); J. Non–Cryst. Sol. **255** 35–121 (1999).
3. D. P. Landau and K. Binder, *A Guide to Monte Carlo Simulations in Statistical Physics* (Cambridge University Press, Cambridge, 2000).
4. S. K. Das, J. Horbach, and K. Binder, J. Chem. Phys. **119**, 1547 (2003).
5. J. P. Hansen and I. R. McDonald, *Theory of Simple Liquids* (Academic Press, London, 1986).
6. J. Horbach, W. Kob, and K. Binder, Phys. Rev. Lett. **88**, 125502 (2002).
7. G. J. Kramer, A. J. M. de Man, R. A. van Santen, J. Am. Chem. Soc. **64**, 6435 (1991).

8. A. Meyer, J. Horbach, W. Kob, F. Kargl, H. Schober, and K. Binder, to be published.
9. R. Weber, Berliner Akad. Wiss. **II**, 1233 (1883); see also A. Bunde, K. Funke, and M. D. Ingram, Solid State Ionics **105**, 1 (1998).
10. J. Habasaki and I. Okada, Molec. Simul. **9**, 319 (1992).
11. H. Knoth, J. Horbach, and K. Binder, to be published.
12. Landolt–Börnstein, *Diffusion in Semiconductors and Non–Metallic Solids*, Vol. 33, Subvolume B1 (Springer, Berlin, 1999).